470 | https://doi.org/10.3311/PPci.38644
Creative Commons Attribution

Periodica Polytechnica Civil Engineering, 69(2), pp. 470–481, 2025

Finite Element Modeling with Ultrasonic Pulse Velocity for Visualising Rock Deformations

Marco A. Navarrete-Seras[1*], Elia. M. Alonso-Guzmán[1,2], Wilfrido Martínez-Molina[1], Hugo L. Chávez-García[1], Mauricio Arreola-Sánchez[1], Jorge A. Borrego-Perez[1], Adrián I. Cervantes-Servín[1]

[1] Faculty of Civil Engineering, Universidad Michoacana de San Nicolas de Hidalgo, Santiago Tapia 403, Col. Centro Histórico, Morelia, Mich. C.P. Morelia 58000, Mexico
[2] Faculty of Architecture, Universidad Michoacana de San Nicolas de Hidalgo, Santiago Tapia 403, Col. Centro Histórico, Morelia, Mich. C.P. Morelia 58000, Mexico
* Corresponding author, e-mail: mnavarrete@umich.mx

Received: 25 October 2024, Accepted: 22 December 2024, Published online: 23 January 2025

Abstract

Rocks serve as critical structural components and aggregates in concrete mixtures for civil infrastructure. A persistent challenge in construction has been the insufficient understanding of the quality of raw materials employed. Non-destructive testing techniques, such as ultrasonic pulse velocity, enable detailed characterization of the physical and mechanical properties of rocks. However, these methods are not consistently applied or accurately interpreted to evaluate rock quality. This study proposes an innovative methodology that integrates ultrasonic pulse velocity to estimate the dynamic modulus of elasticity and assess rock deformation using a finite element model. Ten rock samples, comprising volcanic and crushed rocks, were subjected to analytical techniques. Key parameters, including density, uniaxial compressive strength, and ultrasonic pulse velocity, were measured. Furthermore, advanced methods such as high-resolution scanning electron microscopy and X-ray fluorescence spectroscopy were employed to investigate surface morphology and elemental chemical composition. The findings indicate that crushed materials exhibit superior physical and mechanical properties compared to volcanic stones. The proposed model enables the classification of quarries based on ultrasonic pulse velocity as a physical property and corresponding mechanical properties. The data collected were utilized to calibrate the model for determining the deformability of the rock samples. Numerical analysis revealed strong correlations between ultrasonic pulse velocity and deformation, with a correlation coefficient (R^2) of 0.87 for horizontal deformation and 0.97 for vertical deformation. These results demonstrate that the novel methodology presented in this study provides valuable insights for prioritizing the use of regional quarry materials, thereby supporting the structural integrity of construction projects.

Keywords

rock, finite element, ultrasonic pulse velocity, dynamic modulus of elasticity, deformations

1 Introduction

Rocks are fundamental to modern construction, particularly in applications subjected to elevated loading rates and confining pressures. Serving as primary structural components or as aggregates within ceramic and cementitious matrices, a comprehensive understanding of their physical and mechanical properties is crucial. The growing demand for stone aggregates near urban centres has intensified quarrying activities at city peripheries. However, the absence of systematic experimental analyses and detailed characterization of rock constituents often results in suboptimal material utilization, accelerating the depletion of nearby quarry reserves.

Key indicators of stone quality include density (ρ), uniaxial compressive strength (UCS), and dynamic modulus of elasticity (E_d). These parameters are integral to deformation and displacement models, enabling the selection of optimal materials and quarry sites for efficient rock utilization based on strength characteristics. The mechanical properties, such as UCS, and elastic properties, including E_d and v (Poisson's ratio), play a critical role in engineering design across a wide range of applications, including tunnels, dams, slope stability, and the preservation of historical structures [1]. However, direct testing of rock properties is often challenging, costly, and time-intensive due to the need for high-quality core samples [2, 3].

Cite this article as: Navarrete-Seras, M. A., Alonso-Guzmán, E. M., Martínez-Molina, W., Chávez-García, H. L., Arreola-Sánchez, M., Borrego-Perez, J. A., Cervantes-Servín, A. I. "Finite Element Modeling with Ultrasonic Pulse Velocity for Visualising Rock Deformations", Periodica Polytechnica Civil Engineering, 69(2), pp. 470–481, 2025. https://doi.org/10.3311/PPci.38644

Rocks are characterised through physical (density) and mechanical testing, facilitating the assessment of their behaviour under engineering conditions. Accordingly, specialised research investigates various parameters in rocks, including UCS, as well as static and dynamic E_d. Certain studies utilise techniques such as finite element analysis to model and predict rock behaviour. The presence of disconnected vesicles in extensive basalt flows notably influences properties such as compressive strength, modulus of elasticity, Poisson's ratio, and sonic velocities [4].

Predictive models estimate rock parameters using data such as UCS, E_d, and deformation modulus [5–7]. These models frequently utilise artificial neural networks to predict deformation modulus values [8]. Furthermore, mechanical testing on various volcanic rocks has explored the relationships between chemical and mineralogical composition, microstructure, texture, and physical-mechanical properties [9]. Numerical analyses employing the finite element method have also been conducted to investigate the performance of different adhesives, including cyanoacrylate, polyester, epoxy-based adhesives, and Portland cement paste [10].

The coupled discrete element-finite difference method (DEM-FDM) provides a robust numerical framework for analysing the load-deformation behaviour of soft soils stabilised with columns [11]. DEM has been employed to estimate the elastic properties of damaged rocks [12], while the T-matrix model has demonstrated potential for determining effective stone moduli using the full-wave sonic (FWS) tool [13]. Non-destructive methods have been utilised to characterise stress-induced damage progression in three rock types by capturing their nonlinear elastodynamic responses [14] and overall material behaviour [15]. Additionally, finite element methods (FEM), in conjunction with software such as Abaqus®, have been applied to derive critical rock parameters [16].

Previous studies have explored the relationship between dynamic and static parameters using various methods across different rock types, revealing that discrepancies between dynamic and static elastic moduli are primarily attributable to the presence of microcracks and pores within the rock matrix [17–19]. In another investigation, a laboratory compression test on granite was simulated using the grain-based discrete and finite element method (FDEM). This study examined the brittle fracture process, including damage behaviour initiated by cracking, crack propagation prior to peak failure, and the influence of intrinsic factors such as rock type, grain size distribution, mineralogical composition, and rock texture [20]. Zhou et al. [21] proposed an enriched finite element method for field tests to simulate crack propagation and coalescence in brittle rocks under mixed-mode loading conditions. Furthermore, Wang and Zhou [22] analysed the key characteristics and capabilities of this enriched finite element method, demonstrating its effectiveness in simulating rock failure processes under varying conditions.

Gómez-Heras et al. [23] investigated the combined use of Leeb hardness (LHD) and ultrasonic pulse velocity (UPV) to enhance the estimation of UCS derived from LHD measurements. Their findings demonstrate that this combination significantly improves UCS predictions, particularly when applied to non-porous polymineralic rocks, using portable and non-destructive techniques. Similarly, Pappalardo and Mineo [24] reported that integrating non-destructive V_p (primary wave velocity) measurements with reflectance spectroscopy provides an efficient approach to evaluating the geo-mechanical properties of very weak and weak rock materials. The static elastic modulus of the tested rocks was found to be strongly correlated with UCS and varies according to seismic wave velocities, including both primary V_p and V_s (secondary wave velocity) as well as the dynamic elastic modulus derived from ultrasonic testing.

Although existing studies offer comprehensive analyses of the mechanical and physical properties of rocks, the graphical representation of horizontal and vertical rock deformations remains insufficiently explored. This research introduces a finite element method model to estimate rock sample deformations under applied loads, utilising physical properties such as ultrasonic pulse velocity and density. The model enables a comparative analysis of quarries supplying construction materials in the Morelia region of Michoacán, México. Such advanced quarry characterisation allows for the precise specification of materials, optimising their suitability for diverse construction applications.

2 Methodology

The characterized rock samples were obtained from 10 quarries of stone material located in the surroundings of Morelia (Fig. 1). This corresponds to an average of 11 cubic samples (5 cm × 5 cm × 5 cm) for each type of rock analysed, with a total of 110 samples examined. In this study, the E_d was used for the finite element model (FEM) as it is considered a non-destructive test. As a result, the static modulus of elasticity (E_s) was not obtained. The names of the material quarries stones, sample codes and stone types are given in Table 1.

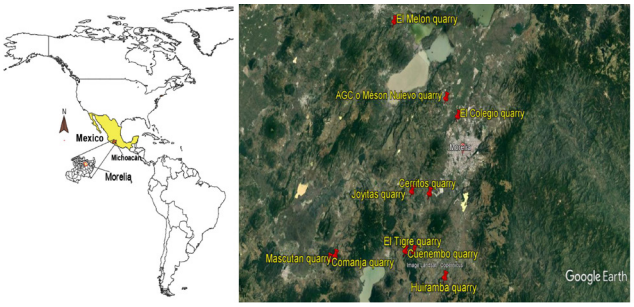

Fig. 1 Location of stone quarries in the surroundings of Morelia, Michoacán, Mexico (Google Earth)

Table 1 Name of the stones, symbology and type of stone analyzed

Quarry number	Quarry name	Symbology	Stone name (Total Alkali–Silica)
1	AGC o Mesón Nuevo	G	Basaltic andesite
2	El Colegio	S	Basaltic andesite
3	Huiramba	H	Trachybasalt
4	Cerritos	C	Basaltic andesite
5	Mascutan	K	Basaltic andesite
6	El Melon	M	Trachybasalt
7	Comanja	CO	Basaltic trachyandesite
8	El Tigre	T	Andesite
9	Cuenembo	CU	Basaltic trachyandesite
10	Joyitas	J	Andesite

Fig. 2 shows the natural rock quarries where rocks are extracted directly from the quarry, as well as crushed rocks, which are extracted in blocks and then crushed before being used in construction. The rocks studied in this research are extrusive igneous rocks. The rocks analysed are part of the Trans-Mexican Volcanic Belt, which showcases extraordinary magmatic diversity influenced by several factors. These include the interaction of two distinct oceanic plates with varying geophysical and compositional properties, the differing intensity of an extensional tectonic regime affecting the upper plate, and a continental basement characterized by diverse ages, thicknesses, and compositions [25].

2.1 Characterization

Characterizations were conducted determine the structural properties of the samples. X-ray fluorescence was performed using ANDREAH equipment. Scanning electron microscope (SEM) was performed using JEOL equipment (leading manufacturer of scientific instrumentation) (model JSM-6400), which has a Bruker X-ray microanalyzer, energy dispersive spectrum (EDS) and the S150A SPUTTER COATER metallizer. The X-ray diffraction was performed by means of a SIEMENS diffractometer, model D5000 X-ray diffractometers, 30 kV, 20 mA at 1.5406 Angstrom wavelength tube.

To determine the physical-mechanical properties, density (ρ) was obtained using a pycnometer, for which the sample was tagged, saturated in water for 24 hours and dried superficially before measurement (ASTM C127-15) [26]. UCS was assessed using the Forney universal testing machine on cubic samples (5 cm × 5 cm × 5 cm) evaluated using Eq. (1).

$$UCS = \frac{P}{A} \tag{1}$$

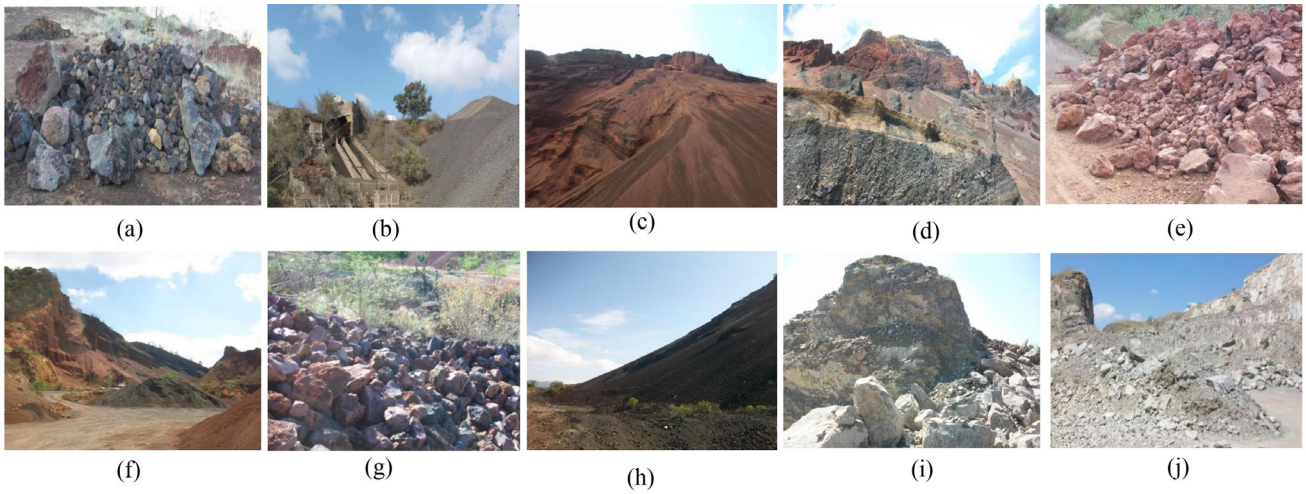

Fig. 2 (a) Huiramba, (b) Joyitas, (c) Maskutan, (d) El Tigre, (e) Comanja, (f) Cuenembo, (g) El Melon, (h) Comanja, (i) AGC, and (j) El Colegio quarries

where UCS is the uniaxial compressive strength (kg_f/cm^2), P is the maximum applied load (kg_f) and A is the cross-sectional area (cm^2) (ASTM D2938-95(2002)) [27, 28].

2.2 Determination of the ultrasonic pulse velocity and E_d

This test is non-destructive, and its main objective is to verify the homogeneity (uniformity and relative quality) of concrete and different construction materials such as rocks. Ultrasonic pulse velocity is the ratio between the travel distance of an ultrasonic wave through the material and the time it takes to traverse it [29].

In rock mechanics, ultrasonic pulse velocity tests are becoming increasingly common due to their non-destructive nature, speed, high precision, and low cost [30].

The dynamic modulus of elasticity was determined by means of ultrasonic pulse velocity using the equipment (model 58E0049/B brand CONTROLS); with a frequency scale from 24 to 150kHz.

Based on ASTM D2845-08, the dynamic modulus of elasticity [31] can be determined by means of Eq. (2).

$$Ed = \rho V_s^2 \left(3V_p^2 - 4V_s^2\right)\frac{V_s^2}{V_p}V_s^2 \tag{2}$$

where E_d is dynamic modulus of elasticity (kg/cm^2), ρ is density (kg/m^3), V_s is secondary wave velocity (m/s) and V_p is primary wave velocity (m/s), based on the work of González De Vallejo and Ferrer [32] for this type of rocks (basalt and andesite), $V_s \approx 2/3\ V_p$.

The Poisson ratio (v) has been estimated in various studies [33–35]. In this research, it was estimated using the Eq. $v = 8\times10^{-09}\left(V_p\right)^2 - 2\times10^{-05}\left(V_p\right) + 0.222$ [36] demonstrates a strong correlation with a coefficient of determination (R^2) of 0.849.

2.3 Modeling

For the development of this model, an almost linear behaviour with local isotropy was taken, for which the governing constitutive equation was proposed (Eq. (3)). Transverse isotropy indicates that at each point in the rock, there is an axis of rotational symmetry. The rock exhibits isotropic properties in the plane perpendicular to this axis, known as the plane of transverse isotropy [37]. Some researchers have studied the influence of igneous rock on seismic images, based on the wave equation that originates from Hooke's law and Newton's second law for isotropic, ideally elastic, heterogeneous [38]. Additionally, other researchers have studied rock masses according to the characteristic of elastic wave propagation in the medium and the application of the elastic wave method in rock mass engineering considering a quasi-isotropic crack mass [39]. In this research the study is performed on the rock matrix therefore it is justified to consider it isotropic as in the aforementioned researches. To estimate the horizontal and vertical displacements based on a four-node element, Eqs. (4)–(6) were used based on the references Kattan (2008), as a generalization of the rectangular four-node element [40]. The stress vector is obtained for each element (Eq. (3)).

$$\{\sigma\} = [D][B]\{u\}, \tag{3}$$

where σ is the stress vector in the element (of size 3 × 1), D is plane stress the matrix and u is the 8 × 1 element displacement vector [40]. For plane stresses, D takes the simple form:

$$D = \frac{E_d}{1-v}\begin{bmatrix} 1 & v & 0 \\ v & 1 & 0 \\ 0 & 0 & \dfrac{1-v}{2} \end{bmatrix}, \tag{4}$$

where E_d is the modulus of elasticity and v is Poisson's ratio. For the basalt and andesite samples, for v an average value of 0.25 was taken based on reference [32, 41]. The isoparametric element stiffness matrix for a bilinear quadrilateral element with sides can then be written as

$$[K]\{U\} = \{F\}, \tag{5}$$

where U is the vector of global nodal displacements, K is the matrix of global stiffnesses and F is the vector of global nodal forces.

To obtain the matrix K, the stiffness matrices of each element (k_1, k_2, k_3, ... k_n) are assembled using Eq. (6).

$$[k] = t\int_{-1}^{1}\int_{-1}^{1}[B]^T[D][B][J]d\xi d\eta, \tag{6}$$

where t is the thickness of the material, D is the matrix of the material properties, J is the Jacobian matrix corresponding to the transformation between the physical and computational spaces. Bi (B_1, B_2, B_3, B_4) are calculated using the bilinear quadrilateral element with natural coordinates of the following Eq. (7) [40].

$$[B] = \frac{1}{|J|}\left[B_1 B_2 B_3 B_4\right], \tag{7}$$

The Eq. (8) is used to obtain Bi (B_1, B_2, B_3, B_4):

$$[B_i]=\begin{bmatrix} a\frac{\partial Ni}{\partial \xi}-b\frac{\partial Ni}{\partial \eta} & 0 \\ 0 & c\frac{\partial Ni}{\partial \eta}-d\frac{\partial Ni}{\partial \xi} \\ c\frac{\partial Ni}{\partial \eta}-d\frac{\partial Ni}{\partial \xi} & a\frac{\partial Ni}{\partial \xi}-b\frac{\partial Ni}{\partial \eta} \end{bmatrix}, \quad (8)$$

where a, b, c, and d are calculated by Eqs. (9)–(12).

$$a=\frac{1}{4}\left[y_1(\xi-1)+y_2(-1-\xi)+y_3(1+\xi)+y_4(1+\xi)\right] \quad (9)$$

$$b=\frac{1}{4}\left[y_1(\eta-1)+y_2(1-\eta)+y_3(1+\eta)+y_4(-1-\eta)\right] \quad (10)$$

$$c=\frac{1}{4}\left[y_1(\eta-1)+y_2(1-\eta)+y_3(1+\eta)+y_4(-1-\eta)\right] \quad (11)$$

$$d=\frac{1}{4}\left[y_1(\xi-1)+y_2(-1-\xi)+y_3(1+\xi)+y_4(1-\xi)\right] \quad (12)$$

The Eqs. (13)–(16) is used to calculate Ni ($N1$, $N2$, $N3$ and $N4$):

$$N1=\frac{1}{4}(1-\xi)(1-\eta) \quad (13)$$

$$N2=\frac{1}{4}(1+\xi)(1-\eta) \quad (14)$$

$$N3=\frac{1}{4}(1+\xi)(1+\eta) \quad (15)$$

$$N4=\frac{1}{4}(1-\xi)(1+\eta) \quad (16)$$

To obtain the Jacobian matrix J the following Eq. (17) is used.

$$|J|=\frac{1}{8}\begin{bmatrix} x_1 & x_2 & x_3 & x_4 \end{bmatrix} \begin{bmatrix} 0 & 1-\eta & \eta-\xi & \xi-1 \\ \eta-1 & 0 & \xi+1 & -\eta-\xi \\ \eta-\xi & -\xi-1 & 0 & \eta+1 \\ 1-\xi & \xi+\eta & -\eta-1 & 0 \end{bmatrix} \begin{bmatrix} y_1 \\ y_2 \\ y_3 \\ y_4 \end{bmatrix} \quad (17)$$

The coordinates were obtained from the bilinear element in the physical coordinate (Fig. 3).

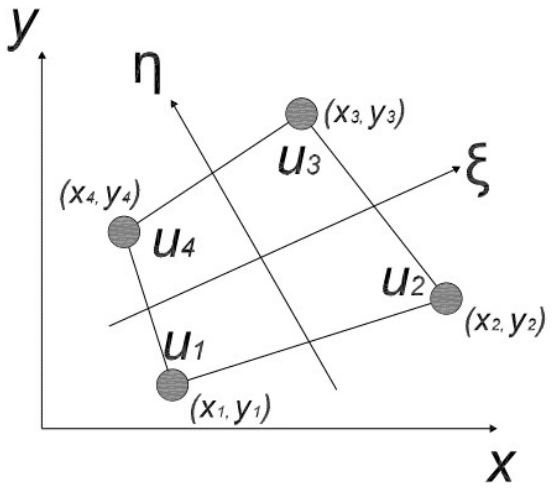

Fig. 3 Bilinear element in physical coordinate

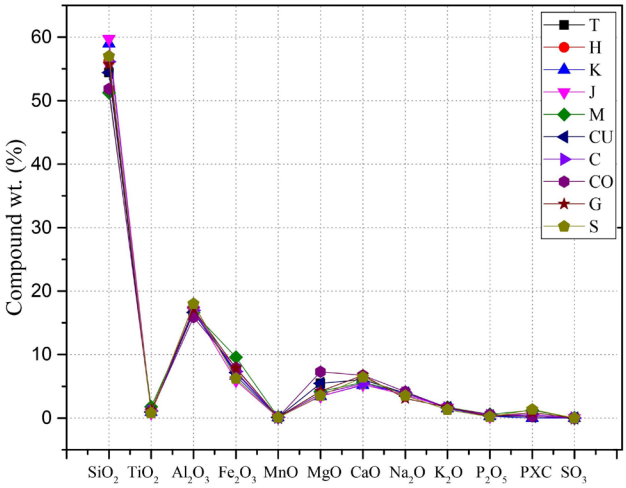

Fig. 4 X-ray fluorescence

3 Results

The results from the X-ray fluorescence characterization performed on all of the samples from the proposed quarries can be seen in Fig. 4. The predominant compound in all samples was SiO_2 (between 50 and 60 %) followed by Al_2O_3 (20%). All the samples present a similarity in the percentages of the compounds, no differences of compounds were observed among the materials. The importance of the above geochemical data allows the chemical classification of rocks and the understanding of the geological process using different types of diagrams. Conventionally, geochemical data used for these purposes are divided into major and trace elements. Major elements are those elements that predominate in any rock such as Si, Ti, Al, Fe, Mn, Mg, Ca, Na and K [42, 43]. With the development of new techniques that allowed the determination of trace and ultra-trace elements, it became essential to determine the chemical composition of rocks over a wide range of concentrations (wt. % to µg g-1) [42].

In this research work, the Total Alkali-Silica (TAS) diagram (Fig. 5) was used, which classifies rocks based on the ratio of SiO_2 wt.% content to the sum of Na_2O wt.% and K_2O wt.% [44, 45]. According to their chemical

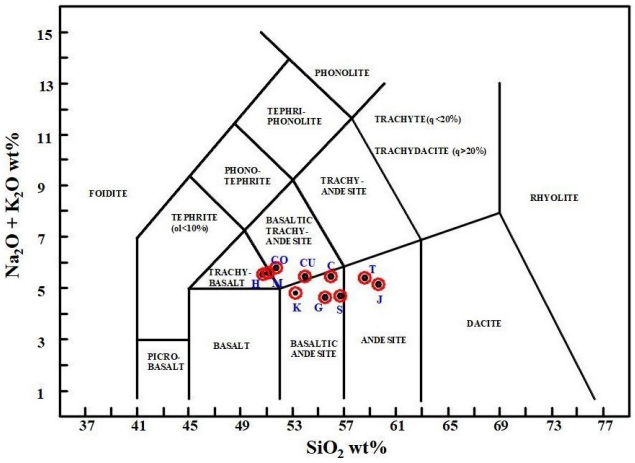

Fig. 5 TAS diagram (Total Alkali-Silica) [44, 45]

composition, quarries G, S, C, and K are classified as basaltic andesite. Quarries CO and CU are categorized as basaltic trachyandesite, while quarries H and M are classified as trachybasalt. Finally, quarries T and J correspond to the classification of andesite.

Figs. 6(a)–(j) shows SEM images of the quarries. The microphotographs reveal substantial changes in pore distribution and size, particularly between volcanic-origin quarries (Figs. 6(a)–(h)) and crushed-origin quarries (Figs. 6(i) and 6(j)). These differences in pore distribution and size directly impact the density and mechanical behaviour of the rocks, particularly affecting the modulus of elasticity, mechanical strength, and results of the ultrasonic pulse velocity test. In the ten images, a distinct change in relief is observed, presenting hollows in most cases; this can be interpreted as the porosity of the material.

The physical and mechanical properties were estimated as outlined in the experimental section. The values for density, uniaxial compressive strength, and modulus of elasticity are shown in Fig. 7. The samples with higher densities, such as G and S, which originate from volcanic material quarries, exhibit higher uniaxial compressive strength. Samples G and S show the highest UCS (110.10 MPa) and density (2567.00 kg/m³), respectively. Volcanic quarries H, C, K, M, CO, T, CU, and J demonstrated lower values in UCS, density, and primary wave velocity (V_p) compared to samples from crushed stone quarries, likely due to the weaker and more abrasive nature of the uncrushed samples. The rock with the lowest Poisson's ratio is H, with a value of 0.21, while the rock with the highest Poisson's ratio is S, with a value of 0.28.

Fig. 8 shows the linear correlation between UCS and E_d for the specimens analysed in this study; the correlation coefficient was R = 0.70, indicating an acceptable correlation [46, 47]. Previous research has validated this

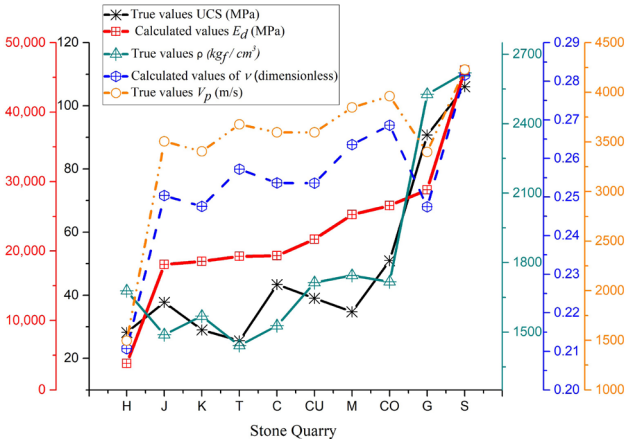

Fig. 7 Density (ρ), uniaxial compressive strength (UCS), primary wave velocity (V_p), Poisson's ratio (v), and dynamic modulus of elasticity (E_d)

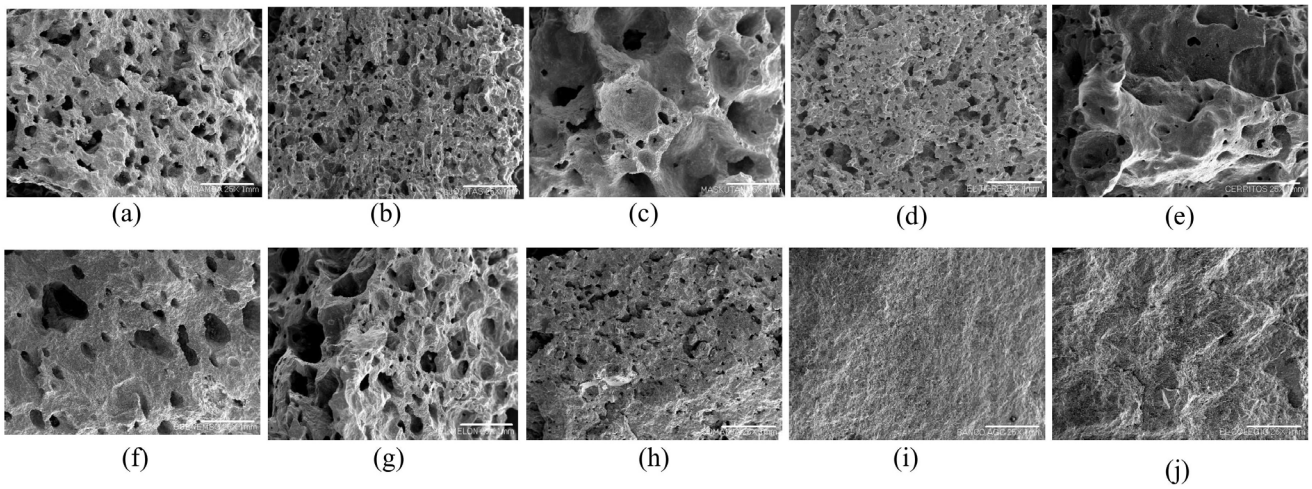

Fig. 6 SEM images of (a) Huiramba, (b) Joyitas, (c) Maskutan, (d) El Tigre, (e) Cerritos, (f) Cuenembo, (g) El Melon, (h) Comanja, (i) AGC, and (j) El Colegio quarries (25 × 1 mm)

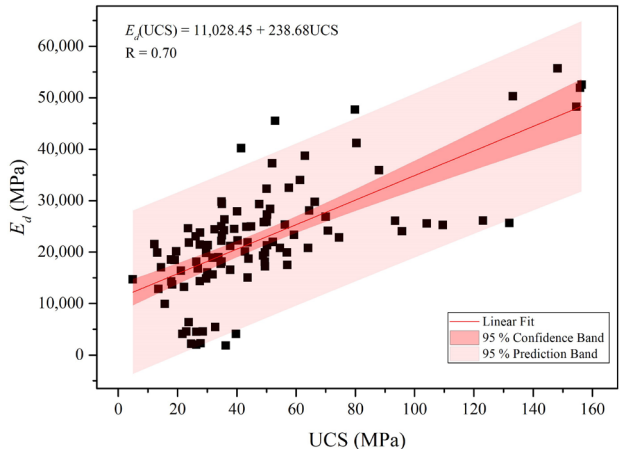

Fig. 8 Correlation between UCS and E_d

correlation between uniaxial compressive strength and dynamic modulus of elasticity [48, 49]. The data presented supports the use of Eqs. (4)–(6) for isotropic materials. This result is related to the degree of rock welding, as the cooling processes of intrusive and extrusive igneous rocks differ. Intrusive rocks exhibit lower porosity (G and S) compared to extrusive ones (H, C, K, M, CO, T, CU, J).

Fig. 9 presents a box-and-whisker plot illustrating the modulus of elasticity of the analysed samples. It is observed that samples from quarry H exhibit the lowest modulus of elasticity, while those from quarry S show the highest modulus. The data dispersion is notable in each quarry, which can be attributed to the different physical and mechanical properties of the studied rocks. Furthermore, this observation is confirmed by the microphotographs presented in Fig. 6, which reveal variability in the porosity of the different rock quarries.

Using the values of maximum applied load and dynamic modulus of elasticity, the equations were discretized and coded in MATLAB with 10,201 nodes per mesh to model

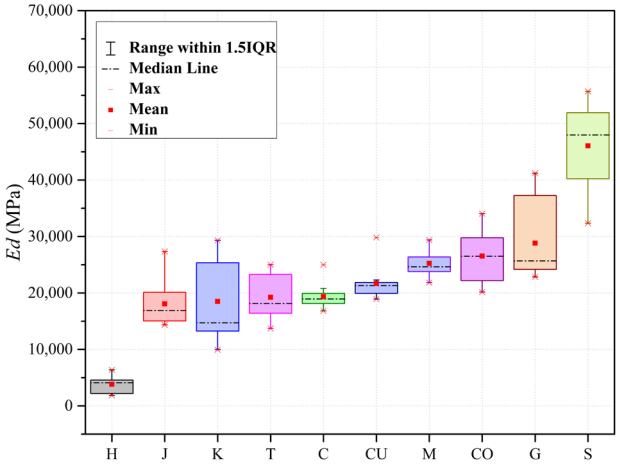

Fig. 9 Modulus of Elasticity of the Rock Quarries

the deformations and displacements. The application of the load at the top was considered, producing values for uniaxial compressive strength, as well as horizontal and vertical displacements. The displacement values obtained were amplified 40 times to better visualize the deformation in the images shown in Fig. 10. The dynamic modulus of elasticity obtained allowed for classifying the rock and estimating its mechanical behaviour.

Fig. 10 shows the 5 cm × 5 cm meshes that represent the profile of each cubic sample, with deformations observed once the maximum load is applied. This data is obtained using the proposed finite element method (FEM) methodology, and the effect of the maximum load on the sample is illustrated by superimposing the undeformed mesh (grey) with the deformed mesh of each sample (blue). The deformations presented in Fig. 10 represent the basaltic andesite rocks (M, C, S, and G). Figs. 10(a) and 10(b) show natural rocks, where minor deformations are observed in samples M, while samples C exhibit greater deformation. Additionally, this classification includes the crushed rocks S and G, whose deformations align with their physical and mechanical properties. Samples S demonstrate a higher ρ, E_d, and UCS compared to sample G. This observation is reflected in Figs. 10(c) and 10(d), where it is evident that rocks S show less deformation.

Fig. 11 presents the deformations of the rocks classified as trachybasalt. It is observed that rocks H exhibit the greatest deformation, further confirming that physical and mechanical properties influence their behaviour. Additionally, samples H recorded the lowest dynamic modulus of elasticity, with a value of 3,813.70 MPa.

Figs. 12 and 13 show the deformations of the rocks classified as basaltic trachyandesite and andesite. In the case of samples C and CU, the deformations are very similar Figs. 12(a) and 12(b). Similarly, the deformations in samples T and J are also comparable to each other Figs. 13(a) and 13(b).

A comparison of the values of the mean displacements (x_{max} and y_{max}) of each stone quarry is observed in Fig. 14. The values in shear stress displacement obtained are equal to less than 0.02 cm similar to those obtained by Vasconcelos and Lourenço that correlated the evolution of vertical displacement with shear displacement in stone masonry with granite blocks, obtaining vertical displacements in the range of −0.6 to 0.3 mm (−0.06 to 0.03 cm) [50].

Table 2 compares the results of the E_d and the Poisson's ratio (v) reported in the literature with those obtained in this research. It was observed that the basaltic andesite from the crushed rocks (S) falls within the E_d range corresponding to basalts. However, the rest of the samples

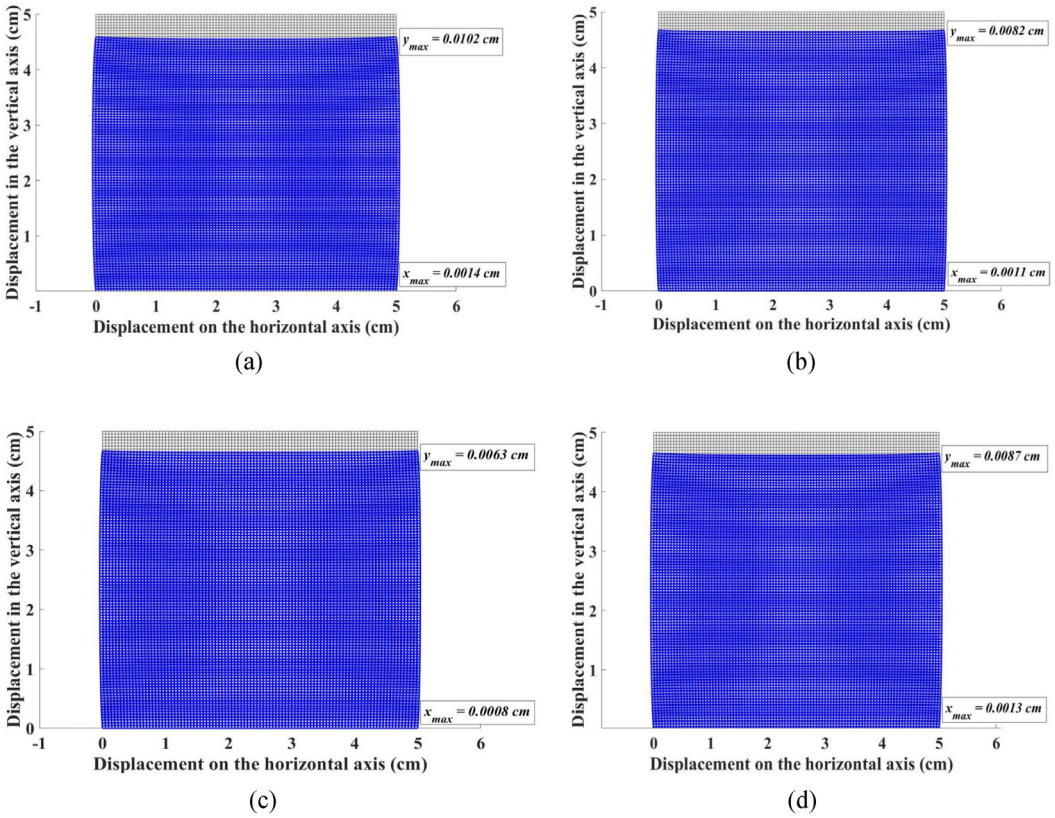

Fig. 10 Deformation of quarry rock basaltic andesite samples: (a) Maskutan, (b) Cerritos, (c) El colegio y (d) AGC

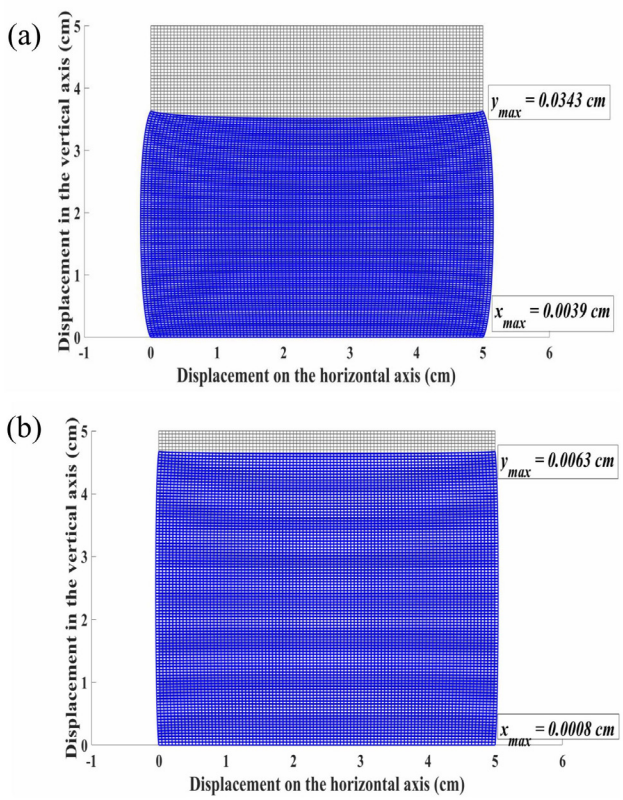

Fig. 11 Deformation of quarry roc trachybasalt samples: (a) Huiramba, and (b) Melon

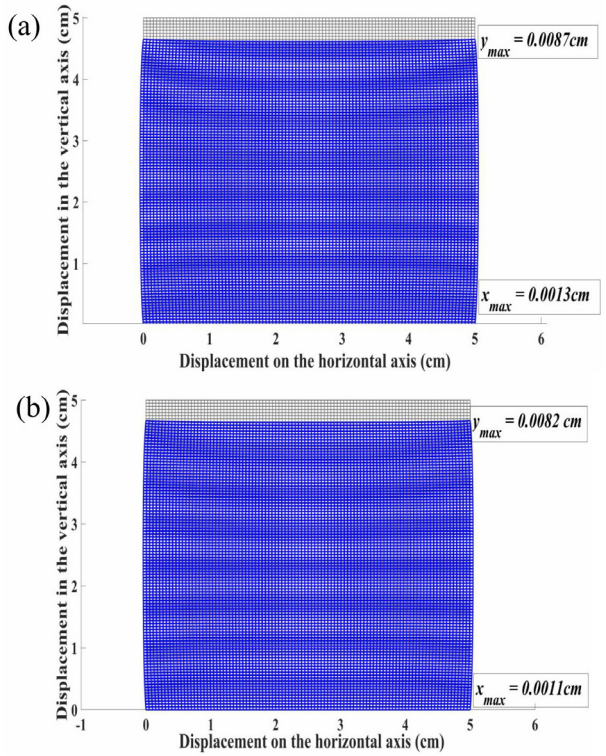

Fig. 12 Deformation of quarry rock basaltic trachyandesite samples: (a) Comanja, and (b) Cuenembo

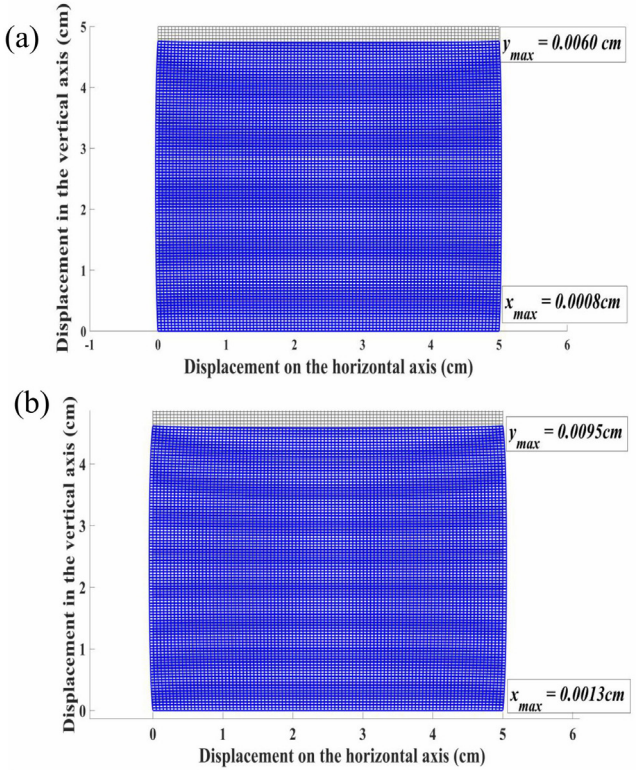

Fig. 13 Deformation of quarry rock andesite samples: (a) El Tigre, and (b) Joyitas

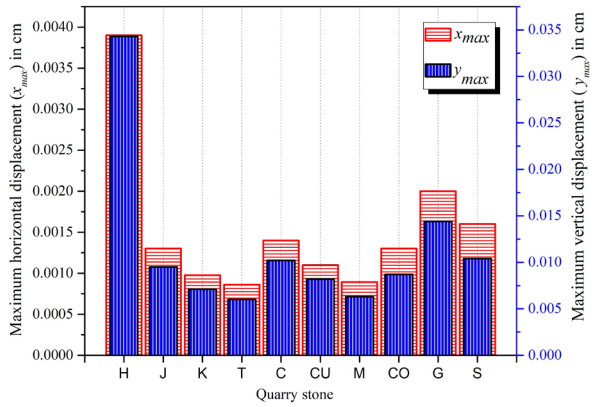

Fig. 14 Displacements horizontal and vertical

exhibit values below 40,000 MPa, confirming that properties such as density (ρ), UCS, and E_d influence their physical-mechanical behaviour, a fact that is supported by the microphotographs shown in Fig. 6.

Additionally, the v values calculated in this research range from 0.21 to 0.28, compared to the range reported in the literature for basalt, which varies from 0.19 to 0.38 [30]. Therefore, the results are within the range of values. Furthermore, to validate the finite element model, the UCS, E_d, and v value ranges for basalt reported in the literature were employed, yielding maximum values (x_{max} and y_{max})

Table 2 Range of E_d, v, x_{max} and y_{max} rocks values

Intact rock	E_d MPa (× 10^4)	Poisson's ratio (v)	x_{max} cm (× 10^{-03})	y_{max} cm (× 10^{-03})
Basalt [32]	4.00 – 8.50	0.19 – 0.38 (0.25)	0.69 – 3.8	6.8 – 17.3
Basaltic Andesite (C, K, S, G)	1.84 – 4.60	0.25 – 0.28	0.98 – 2.00	7.10 – 4.40
Trachybasalt (H, M)	0.38 – 2.52	0.21 – 0.26	0.89 – 3.90	6.30 – 34.3
Basaltic trachyandesite (CO, CU)	2.17 – 2.65	0.25 – 0.27	1.10 – 1.30	8.20 – 8.70
Andesite (T, J)	1.81 – 1.92	0.25 – 0.26	0.86 – 1.30	6.00 – 9.50

Maximum and minimum values. Average values in parentheses.

that demonstrate that the deformations are very similar to those observed in the rocks studied in this research.

Fig. 15 illustrates the correlation between the propagation V_p and the maximum displacements at x_{max} and y_{max}. Second-degree polynomials were fitted to the data, resulting in acceptable correlation coefficients. These results support the validity of the mathematical model for estimating deformations in rock samples and its utility as a primary or preliminary classification tool for rocks used in civil engineering construction. The error of the sum of squares for polynomial fit of x_{max} is 9.64 × 10^{-7} and the error of the sum of squares for polynomial fit y_{max} is 4.56 x 10^{-5}.

4 Conclusions

Different samples of stone quarries used for construction at the study site were analysed. Physical and mechanical tests were performed, and the values of density, modulus

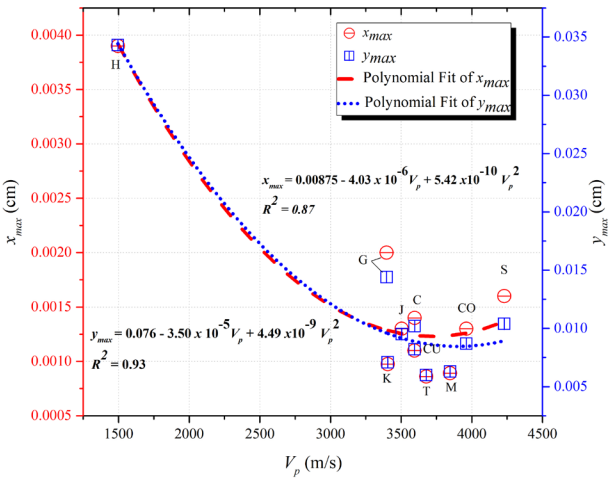

Fig. 15 Correlation of V_p versus deformation in x_{max} and y_{max}

of elasticity, and uniaxial compressive strength were compared. Results from the model showed a clear difference between the crushed and volcanic quarry samples (average crushed samples E_d = 37,433.10 MPa compared to average volcanic samples E_d = 19,051.82 MPa).

It was determined that the greatest deformation occurred in the natural rock quarry H ($x_{max} = 3.9 \times 10^{-3}$ cm and $y_{max} = 34.3 \times 10^{-3}$ cm), classified as trachybasalt, while the smallest deformation corresponded to the rock quarry T ($x_{max} = 0.86 \times 10^{-3}$ cm and $y_{max} = 6 \times 10^{-3}$ cm), classified as andesite. In the analysis of crushed rocks, quarry S exhibited lower deformation compared to quarry G, both classified as basaltic andesite. This study revealed that physical-mechanical properties, such as the propagation velocity of P-waves (V_p), dynamic modulus of elasticity (E_d), and uniaxial compressive strength (UCS), significantly influence the maximum (x_{max}) and minimum (y_{max}) deformation behaviour of each analysed quarry. In conclusion, the results of the analysis indicate that geological classification and the physical-mechanical properties of rocks are determining factors in deformation behaviour. The variability observed among the quarries suggests that a detailed understanding of these characteristics is essential for the proper selection of materials in engineering applications.

The classification of rocks using the Total Alkali-Silica (TAS) diagram, X-ray fluorescence, and scanning electron microscopy (SEM) are fundamental tools in this research. These techniques allow for validation and certainty in the finite element model, supported by ultrasonic pulse velocity, which facilitates the visualization of deformations in the quarries, thereby expanding the tools for accurate rock classification that can jointly employ chemical and physical-mechanical characteristics.

The mathematical model proposed in this work can be applied to understand the deformations of stones used in other regions and to determine the stone quarries with the best properties for construction use (Aggregates for hydraulic concrete blends, asphalt pavements, masonry, and foundations). The application of this methodology could aid decision-makers by identifying unexploited quarries that meet construction requirements, thus preventing the overexploitation of currently operational quarries.

Acknowledgement

Authors would like to thank the financial support of: "Coordinación de Investigación Científica, CIC, de Universidad Michoacana de San Nicolas de Hidalgo, UMSNH. Secretaría de Educación Pública, SEP. Programa Prodep; Consejo Nacional de Humanidades, Ciencia y Tecnología, CONHACYT Protocols 315660 and 315680" and "Programa Estancias Posdoctorales por México" (J. A. Borrego Pérez CVU:460429); and "Programa de Becas de Movilidad Académica entre Instituciones Asociadas a la Asociación Universitaria Iberoamericana de Posgrado". Additionally, the authors are grateful to the technical support received from the "Ing. Luis Silva Ruelas" laboratory staff at the UMSNH Faculty of Civil Engineering.

References

[1] Yao, W., Xia, K. "Dynamic notched semi-circle bend (NSCB) method for measuring fracture properties of rocks: Fundamentals and applications", Journal of Rock Mechanics and Geotechnical Engineering, 11(5), pp. 1066–1093, 2019. https://doi.org/10.1016/j.jrmge.2019.03.003

[2] Shalabi, F. I., Cording, E. J., Al-Hattamleh, O. H. "Estimation of rock engineering properties using hardness tests", Engineering Geology, 90(3–4), pp. 138–147, 2007. https://doi.org/10.1016/j.enggeo.2006.12.006

[3] Ocak, I. "Estimating the modulus of elasticity of the rock material from compressive strength and unit weight", Journal of the Southern African Institute of Mining and Metallurgy, 108(10), pp. 621–626, 2008.

[4] Al-Harthi, A. A., Al-Amri, R. M., Shehata, W. M. "The porosity and engineering properties of vesicular basalt in Saudi Arabia", Engineering Geology, 54(3–4), pp. 313–320, 1999. https://doi.org/10.1016/S0013-7952(99)00050-2

[5] Aboutaleb, S., Behnia, M., Bagherpour, R., Bluekian, B. "Using non-destructive tests for estimating uniaxial compressive strength and static Young's modulus of carbonate rocks via some modeling techniques", Bulletin of Engineering Geology and Environment, 77(4), pp. 1717–1728, 2018. https://doi.org/10.1007/s10064-017-1043-2

[6] Aladejare, A. E., Akeju, V. O., Wang, Y. "Data-driven characterization of the correlation between uniaxial compressive strength and Youngs' modulus of rock without regression models", Transportation Geotechnics, 32, 100680, 2022. https://doi.org/10.1016/j.trgeo.2021.100680

[7] Fang, Z., Qajar, J., Safari, K., Hosseini, S., Khajehzadeh, M., Nehdi, M. L. "Application of Non-Destructive Test Results to Estimate Rock Mechanical Characteristics—A Case Study", Minerals, 13(4), 472, 2023. https://doi.org/10.3390/min13040472

[8] Haghnejad, A., Ahangari, K., Noorzad, A. "Investigation on Various Relations Between Uniaxial Compressive Strength, Elasticity and Deformation Modulus of Asmari Formation in Iran", Arabian Journal for Science and Engineering, 39(4), pp. 2677–2682, 2014. https://doi.org/10.1007/s13369-014-0960-7

[9] Pola, A., Crosta, G. B., Fusi, N., Castellanza, R. "General characterization of the mechanical behaviour of different volcanic rocks with respect to alteration", Engineering Geology, 169, pp. 1–13, 2014. https://doi.org/10.1016/j.enggeo.2013.11.011

[10] Komurlu, E., Cihangir, F., Kesimal, A., Demir, S. "Effect of Adhesive Type on the Measurement of Modulus of Elasticity Using Electrical Resistance Strain Gauges", Arabian Journal for Science and Engineering, 41(2), pp. 433–441, 2016. https://doi.org/10.1007/s13369-015-1837-0

[11] Indraratna, B., Ngo, N. T., Rujikiatkamjorn, C., Sloan, S. W. "Coupled discrete element–finite difference method for analysing the load-deformation behaviour of a single stone column in soft soil", Computers and Geotechnics, 63, pp. 267–278, 2015. https://doi.org/10.1016/j.compgeo.2014.10.002

[12] Abe, S. "Comparison of discrete element simulations to theoretical predictions of the elastic moduli of damaged rocks", International Journal Rock Mechanics and Mining Sciences, 88, pp. 265–272, 2016. https://doi.org/10.1016/j.ijrmms.2016.07.022

[13] Chalupa, F., Vilhelm, J., Petruzálek, M., Bukovská, Z. "Application of T-matrix model for static moduli approximation from dynamic moduli determined by sonic well logging", International Journal of Rock Mechanics and Mining Sciences, 112, pp. 81–289, 2018. https://doi.org/10.1016/j.ijrmms.2018.10.031

[14] Shirole, D., Walton, G., Ostrovsky, L., Masoumi, H., Hedayat, A. "Non-linear ultrasonic monitoring of damage progression in disparate rocks", International Journal of Rock Mechanics and Mining Sciences, 111, pp. 33–44, 2018. https://doi.org/10.1016/j.ijrmms.2018.08.010

[15] Coli, M., Ciuffreda, A. L., Donigaglia, T. "Technical Analysis of the Masonry of the Bargello' Palace, Florence (Italy)", Applied Sciences, 12(5), 2615, 2022. https://doi.org/10.3390/app12052615

[16] Zoccali, P., Moretti, L., Di Mascio, P., Loprencipe, G., D'Andrea, A., Bonin, G., Teltayev, B., Caro, S. "Analysis of natural stone block pavements in urban shared areas", Case Studies in Constructions Materials, 8, pp. 498–506, 2018. https://doi.org/10.1016/j.cscm.2018.04.004

[17] Azimian, A., Ajalloeian, R. "Empirical correlation of physical and mechanical properties of marly rocks with P wave velocity", Arabian Journal of Geosciences, 8(4), pp. 2069–2079, 2015. https://doi.org/10.1007/s12517-013-1235-4

[18] Shen, S., Gao, Y., Jia, L. "A Comparison of the Relationship between Dynamic and Static Rock Mechanical Parameters", Applied Sciences, 14(11), 4487, 2024. https://doi.org/10.3390/app14114487

[19] Davarpanah, S. M., Ván, P., Vásárhelyi, B. "Investigation of the relationship between dynamic and static deformation moduli of rocks", Geomechanics and Geophysics for Geo-Energy and Geo-Resources, 6(1), 29, 2020. https://doi.org/10.1007/s40948-020-00155-z

[20] Li, X. F., Li, H. B., Liu, L. W., Liu, Y. Q., Ju, M. H., Zhao, J. "Investigating the crack initiation and propagation mechanism in brittle rocks using grain-based finite-discrete element method", International Journal of Rock Mechanics and Mining Sciences, 127, 104219, 2020. https://doi.org/10.1016/j.ijrmms.2020.104219

[21] Zhou, X., Jia, Z., Wang, L. "A field-enriched finite element method for brittle fracture in rocks subjected to mixed mode loading", Engineering Analysis with Boundary Elements, 129, pp. 105–124, 2021. https://doi.org/10.1016/j.enganabound.2021.04.023

[22] Wang, L.-F. Zhou, X.-P. "A field-enriched finite element method for simulating the failure process of rocks with different defects", Computers & Structures, 250, 106539, 2021. https://doi.org/10.1016/j.compstruc.2021.106539

[23] Gómez-Heras, M., Benavente, D., Pla, C., Martinez-Martinez, J., Fort, R., Brotons, V. "Ultrasonic pulse velocity as a way of improving uniaxial compressive strength estimations from Leeb hardness measurements", Construction and Building Materials, 261, 119996, 2020. https://doi.org/10.1016/j.conbuildmat.2020.119996

[24] Pappalardo, G. Mineo, S. "Static elastic modulus of rocks predicted through regression models and Artificial Neural Network", Engineering Geology, 308, 106829, 2022. https://doi.org/10.1016/j.enggeo.2022.106829

[25] Gómez-Tuena, A., Orozco-Esquivel, M. T., Ferrari, L. "Igneous petrogenesis of the Trans-Mexican Volcanic Belt", In: Alaniz-Álvarez, S. A., Nieto-Samaniego, Á. F. (eds.) Geology of México: Celebrating the Centenary of the Geological Society of México, Geological Society of America, 2007, pp. 129–182. ISBN: 9780813724225 https://doi.org/10.1130/2007.2422(05)

[26] American Society for Testing Materials "ASTM C127-15, Standard Test Method for Laboratory Method for Density, Relative Density (Specific Gravity), and Absorption of Coarse Aggregate (Withdrawn 2024)", ASTM, West Conshohocken, PA, USA, 2015. https://doi.org/10.1520/C0127-15

[27] American Society for Testing Materials "ASTM D2938-95(2002), Standard Test Method for Unconfined Compressive Strength of Intact Rock Core Specimens (Withdrawn 2005)", ASTM, West Conshohocken, PA, USA, 2002.

[28] Navarro, L., Martínez, W., Espinoza, A. "Análisis de Materiales, Manual de Análisis de Materiales, Resistencia de Materiales" (Materials Analysis, Manual of Materials Analysis, Strength of Materials), Universidad Michoacana de San Nicolás de Hidalgo, 2011. (in Spanish)

[29] Rincón, O. T., Carruyo, A. R., Andrade, C., Helene, P. R. L., Díaz, I. (eds.) "Manual de Inspección, Evaluación y Diagnostico de Corrosión En Estructuras de Hormigón Armado" (Manual for Inspection, Evaluation and Diagnosis of Corrosion in Reinforced Concrete Structures), CYTED, 1998. ISBN: 980-296-541-3 (in Spanish)

[30] Chawre, B. "Correlations between ultrasonic pulse wave velocities and rock properties of quartz-mica schist", Journal of Rock Mechanics and Geotechnical Engineering, 10(3), pp. 594–602, 2018. https://doi.org/10.1016/j.jrmge.2018.01.006

[31] American Society for Testing Materials "ASTM D2845-08, Standard Test Method for Laboratory Determination of Pulse Velocities and Ultrasonic Elastic Constants of Rock (Withdrawn 2017)", ASTM, West Conshohocken, PA, USA, 2008.

[32] González De Vallejo, L.-I., Ferrer, M. "Geological Engineering", CRC Press, 2011. ISBN: 9780429065491 https://doi.org/10.1201/b11745

[33] Dong, L., Xu, H., Fan, P., Wu, Z. "On the Experimental Determination of Poisson's Ratio for Intact Rocks and Its Variation as Deformation Develops", Advances in Civil Engineering, 2021(1), 2021. https://doi.org/10.1155/2021/8843056

[34] Rezaei, M., Davoodi, P. K., Najmoddini, I. "Studying the correlation of rock properties with P-wave velocity index in dry and saturated conditions", Journal of Applied Geophysics, 169, pp. 49–57, 2019. https://doi.org/10.1016/j.jappgeo.2019.04.017

[35] Khandelwal, M. Singh, T. N. "Correlating static properties of coal measures rocks with P-wave velocity", International Journal of Coal Geology, 79(1–2), pp. 55–60, 2009. https://doi.org/10.1016/j.coal.2009.01.004

[36] Khandelwal, M. "Correlating P-wave Velocity with the Physico-Mechanical Properties of Different Rocks", Pure and Applied Geophysics, 170(4), pp. 507–514, 2013. https://doi.org/10.1007/s00024-012-0556-7

[37] Hakala, M., Kuula, H., Hudson, J. A. "Estimating the transversely isotropic elastic intact rock properties for in situ stress measurement data reduction: A case study of the Olkiluoto mica gneiss, Finland", International Journal of Rock Mechanics and Mining Sciences, 44(1), pp. 14–46, 2007. https://doi.org/10.1016/j.ijrmms.2006.04.003

[38] Sun, D., Shi, X., Wang, Z., Chen, L., Wang, J., Sun, J., Dai, D., Fang, Q. "Influences of Permian igneous rock on seismic imaging of underlying strata in the Hanilcatam area, Tarim Basin, China", Journal of Natural Gas Geoscience, 4(1), pp. 71–77, 2019. https://doi.org/10.1016/j.jnggs.2019.03.004

[39] Wang, H., Jia, J., Li, X., Xian, X., Hu, G. "Cranny density parameters and porosity measured by elastic wave method in quasi-isotropic cranny rock masses", Journal of Central South University of Technology, 13(5), pp. 598–602, 2006. https://doi.org/10.1007/s11771-006-0095-4

[40] Kattan, P. I. "The Plane Truss Element", In: MATLAB Guide to Finite Elements: An Interactive Approach, Springer Berlin, Heidelberg, 2008, pp. 61–89. ISBN: 978-3-540-70697-7 https://doi.org/10.1007/978-3-540-70698-4_5

[41] Lógó, B. A., Vásárhelyi, B. "Estimation of the Poisson's Rate of the Intact Rock in the Function of the Rigidity", Periodica Polytechnica Civil Engineering, 63(4), pp. 1030–1037, 2019. https://doi.org/10.3311/PPci.14946

[42] Rollinson, H. R. "Using Geochemical Data", Routledge, 2014. ISBN: 9781315845548 https://doi.org/10.4324/9781315845548

[43] Geisenblosen, M. C., Oyhantçabal, P., Pistón, M. "Determination of major elements in igneous rocks using microwave plasma atomic emission spectrometry (MP-AES)", MethodsX, 9, 101793, 2022. https://doi.org/10.1016/j.mex.2022.101793

[44] Le Maitre, R. W. "A proposal by the IUGS Subcommission on the Systematics of Igneous Rocks for a chemical classification of volcanic rocks based on the total alkali silica (TAS) diagram", Australian Journal of Earth Sciences, 31(2), pp. 243–255, 1984. https://doi.org/10.1080/08120098408729295

[45] Bas, M. J. L., Le Maitre, R. W., Streckeisen, A., Zanettin, B. "A Chemical Classification of Volcanic Rocks Based on the Total Alkali-Silica Diagram", Journal of Petrology, 27(3), pp. 745–750, 1986. https://doi.org/10.1093/petrology/27.3.745

[46] Figeroa Montaño, A., Ramírez Sánchez, H. U., Alcalá Gutiérrez, J. "Introducción a la metodología experimental" (Introduction to experimental methodology), Pearson Educación, 2014. ISBN: 978-607-32-2222-8 (in Spanish)

[47] Silva, A., de Brito, J., Gaspar, P. L. "Methodologies for Service Life Prediction of Buildings with a Focus on Façade Claddings", Springer Cham, 2016. ISBN: 978-3-319-33288-8 https://doi.org/10.1007/978-3-319-33290-1

[48] Majstorović, J., Gligorić, M., Lutovac, S., Negovanović, M., Crnogorac, L. "Correlation of uniaxial compressive strength with the dynamic elastic modulus, P - wave velocity and S - wave velocity of different rock types", Podzemni Radovi, 2019(34), pp. 11–25, 2019. https://doi.org/10.5937/PodRad1934011M

[49] Najibi, A. R., Ghafoori, M., Lashkaripour, G. R., Asef, M. R. "Empirical relations between strength and static and dynamic elastic properties of Asmari and Sarvak limestones, two main oil reservoirs in Iran", Journal of Petroleum Science and Engineering, 126, pp. 78–82, 2015. https://doi.org/10.1016/j.petrol.2014.12.010

[50] Vasconcelos, G., Lourenço, P. B. "Experimental characterization of stone masonry in shear and compression", Construction and Building Materials, 23(11), pp. 3337–3345, 2009. https://doi.org/10.1016/j.conbuildmat.2009.06.045